applied optics

Traveling tunable laser projector for UV-blue disinfection dose determinations

Thomas Larason,[1,*] Steven Grantham,[1] Clarence Zarobila,[1] Yuqin Zong,[1] Michael Schuit,[2] Brian Holland,[2] Stewart Wood,[2] Melissa Krause,[2] and C. Cameron Miller[1]

[1]U.S. Department of Commerce, National Institute of Standards and Technology, Gaithersburg, Maryland 20899, USA
[2]U.S. Department of Homeland Security (DHS) Science and Technology Directorate (S&T), National Biodefense Analysis and Countermeasures Center, Battelle National Biodefense Institute (BNBI), Frederick, Maryland 21702, USA
*Corresponding author: thomas.larason@nist.gov

Received 4 April 2022; revised 3 June 2022; accepted 7 June 2022; posted 8 June 2022; published 21 June 2022

As the COVID-19 pandemic was overtaking the world in the spring of 2020, the National Institute of Standards and Technology (NIST) began collaborating with the National Biodefense Analysis and Countermeasures Center to study the inactivation of SARS-CoV-2 after exposure to different ultraviolet (UV) and blue light wavelengths. This paper describes a 1 kHz pulsed laser and projection system used to study the doses required to inactive SARS-CoV-2 over the wavelength range of 222 to 488 nm. This paper builds on NIST's previous work for water pathogen inactivation using UV laser irradiation. The design of the laser and projection system and its performance in a Biosafety Level 3 (BSL-3) laboratory are given. The SARS-CoV-2 inactivation results (published elsewhere by Schuit, M.A., *et al*., expected 2022) demonstrate that a tunable laser projection system is an invaluable tool for this research.

https://doi.org/10.1364/AO.460317

1. INTRODUCTION

Healthcare-associated infections (HAI) are one of the leading causes of death in the United States. While HAI statistics are difficult to ascertain, according to the US Centers for Disease Control and Prevention (CDC) records, nationwide, HAIs infect about one in every 25 hospital patients [1]. This ratio translates into approximately 1.7 million HAIs occurring in US hospitals, resulting in nearly 100,000 or more unnecessary deaths, costing an estimated 20 billion in US dollars [2]. The deaths from HAIs place HAI deaths nearly at the level of those attributed to Alzheimer's disease and above the seventh leading cause of death in the US, diabetes [3]. In addition, viral, bacterial, and fungal resistance continue to emerge while parasites, zoonotic pathogens, and major shifts in traditional respiratory pathogens continue to create challenges. The public outbreak of SARS-CoV-2 and the efficiency of transmission for any respiratory virus has important implications for containment and mitigation strategies [4]. COVID-19 is not only a new biological concern [4], but it has also substantially impacted traditional HAI surveillance and prevention efforts [5].

A potential tool in the fight against HAIs is germicidal ultraviolet (GUV) disinfection. GUV refers to the UVC wavelength range of 200 to 280 nm. A variety of GUV radiation sources are available including low-pressure mercury discharge tubes, excimer lamps, and light-emitting diodes (LED). Radiation in the wavelength range of 200 to 280 nm is absorbed by proteins, deoxyribonucleic acid (DNA), and ribonucleic acid (RNA), which may lead to damage and loss of functionality [6]. This germicidal activity was discovered more than 100 years ago by the Danish physician Niels Finsen, who would receive the 1904 Nobel Prize in Medicine for his discovery [6].

GUV devices come in a variety of sizes and formats. Certain units are permanently installed and used to treat rooms or may be installed in air ducts and used to disinfect airborne pathogens. Others are mobile units on wheels, large enough to treat an entire hospital room. Smaller units, the size of a microwave oven, are used to disinfect cell phones and operating instruments. All rely on the UVC irradiating the pathogen, at a known intensity, from a certain distance for a certain amount of time, to achieve the desired results.

Hundreds of studies have been completed on a multitude of pathogens to determine the amount of UV radiation that is required to inactivate them [7]. The challenge in comparing these studies is that environmental conditions vary. In order to develop a better understanding of the effects of environmental conditions on the effectiveness of UV inactivation, a standard condition is required. For example, if the pathogen is exposed in distilled water or droplets of distilled water that have been allowed to dry on a surface and standard model for fluid absorbance adjustment factors are calculated (for example, the method of Bolton and Linden for calculating dose adjustment "water factor" values [8]), the direct effects of the UV radiation can be ascertained. NIST has previously demonstrated a laser-based system that allowed the UV wavelength dependence to be

measured [9]. In a rapid response to the COVID-19 pandemic, NIST researchers along with the National Biodefense Analysis and Countermeasures Center researchers have improved this system by coupling it to an optical fiber which facilitated use of the source in a biocontainment laboratory. These improvements will be the focus of this paper.

2. TRAVELING TUNABLE LASER PROJECTOR

A. Laser Subsystem: Laser and Launch Box

The NIST traveling tunable laser projector (TTLP) is comprised of two optical subsystems connected by a optical fiber. The laser subsystem remained outside of the Biosafety Level 3 (BSL-3) laboratory. Taking the subsystem into a biocontainment facility would have required a gaseous decontamination (e.g., with vaporized hydrogen peroxide) to remove the subsystem safely, which may result in substantial damage to the components of this subsystem. The laser subsystem consisted of an Ekspla NT242-SH-SFG 1 kHz optical parametric oscillator (OPO) pulsed (class 4) laser [9] and optics for coupling the laser beam into an optical fiber as shown in Fig. 1

All the optics outside of the laser are enclosed in a light-tight box referred to as the "launch box." A photograph of the laser subsystem and auxiliary equipment in the hallway outside the BSL-3 lab is shown in Fig. 2.

For this study, the monochromatic wavelengths produced by the laser were: 222, 230, 240, 253.7, 260, 270, 280, 290, 300, 305, 315, 325, 365, 405, 450, and 488 nm. The wavelengths in the UVC and UVB region were chosen to be equally spaced except for 222 nm and 253.7 nm, which are the common wavelengths produced by commercial sources, excimer and low-pressure mercury lamps, respectfully. The wavelengths 365 nm and 405 nm were chosen because they are the wavelengths produced by medium pressure mercury lamps. Additionally, very efficient LEDs are available at these two wavelengths because 365 nm is used in manufacturing and 405 nm is used in Blu-ray players. Other commonly available sources are at the wavelengths of 450 nm (diode lasers) and 488 nm (argon-ion lasers).

Referring to Figs. 1(a) and 1(b) one can see that inside the launch box the laser beam first passes through two shutters upon exiting the laser housing. The first shutter is a "safety" shutter, which totally blocks any light from escaping from the laser housing. It is controlled by hard-wired safety shutoff switches at both subsystem locations (i.e., outside and inside the BSL-3 lab). The second shutter controls the time interval for which the samples are exposed to the laser light.

Next, the laser beam is directed into a Pellin–Broca prism [10] (Thorlabs ADBU-20) and aperture to block the out-of-band radiation. A turning mirror then directs the beam through a 75 mm focal length UV fused silica, plano-convex lens (Telaztec L32-RAR-S) to focus light into the optical fiber. Changes in the laser wavelength requires only a small manual rotation of the prism to adjust the output angle. The chromatic focal shift in the focusing lens requires no adjustment once optimized. This is due to the large fiber core diameter (1.5 mm), which accepts the focused beam over the wavelength range of this study.

The custom optical fiber (Armadillo Sia, Optran UVNSS 1500/1590/1615/2000 CPF) was securely installed under a door and carried the laser beam to the projector subsystem. Two optical fiber lengths were used during this study. A 5 m optical fiber was first used to direct light from the laser system into the lab. However, after installing the laser system, a 4 m optical fiber was found to be of adequate length and reduced the loss due to the fiber transmission and solarization losses. Most of the wavelengths examined used the 4 m optical fiber.

B. Projection Subsystem

The projection subsystem contains the optics for expanding and directing the laser beam onto the study samples as shown in Fig. 3. This subsystem was placed inside a biological safety cabinet (BSC) in the BSL-3 lab. Figure 4 shows the projector installed in the BSC.

Within the BSL-3 lab, the projection subsystem manipulates the fiber output with an engineered diffuser-based system to produce a uniform beam. The projection system and the output cone are fully enclosed in a 3D printed polyethylene terephthalate glycol (PETG) enclosure and shroud (shown in Fig. 3) to fully contain the projector's output and provide exposure protection for BSL-3 lab staff. A beam splitter tilted at 45° within the projector provides a low loss pick off to monitor the projector's throughput. Two UV detectors and two visible detectors measured the exposures. One of each was used as the monitor detector, which continuously measured the laser during the sample exposures.

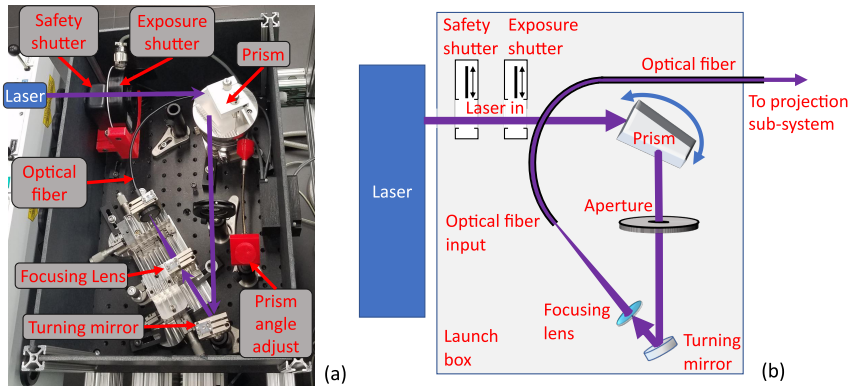

Fig. 1. Optical layout of fiber coupling optics in the launch box. (a) Photograph of the launch box and (b) schematic diagram.

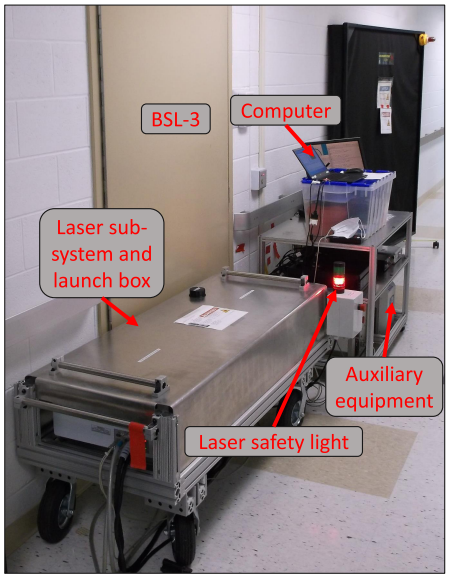

Fig. 2. Photograph of the laser subsystem and auxiliary equipment in the hallway outside the BSL-3 lab.

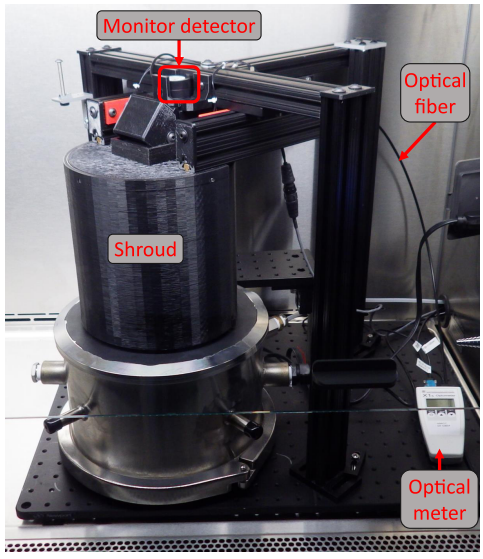

Fig. 3. Photograph of projection sub-system in the BCS.

Due to the limited volume of space available in the BSC, the projection system was designed to be simple, with a minimum number of components. Only those components necessary to project a spot of the desired size with reasonable uniformity were used. Figure 5 shows a schematic layout of the setup without its mechanical support structures. The distance between the optical axis of the projector and the plane containing the study samples is 279 mm. UV radiation propagates from left to right, then downward to the sample area after reflection by the fold mirror.

After exiting the optical fiber, the light is collected and collimated with an uncoated fused-silica 12.7 mm diameter plano-convex collimating lens (Thorlabs LA4647). Its first surface is located about 19 mm from the optical fiber face. A fused silica engineered diffuser (RPC Photonics EDC-10-G-1R) is positioned 25 mm after the collimating lens and is used to homogenize and scatter UV radiation into a maximum angle dependent on the diffuser design angle. The uniformity at the sample plane is highly dependent on the diffusing angle, so a variety of diffusers having different diffusing angles were investigated, including 1°, 5°, 10°, and 20°; ultimately, the 10° diffusing angle was chosen to balance uniformity with maximum irradiance. UV radiation from the diffuser floods an 8 mm diameter aperture located 25 mm after the diffuser. The aperture is the object to be imaged by an uncoated fused silica 12.7 mm diameter projector lens (Thorlabs LA4936). The focal length of the lens (30.1 mm) was selected so that a nominal 100 mm diameter image of the aperture was projected onto the sample plane. The projector lens to aperture separation was adjusted from the nominal 26.6 mm separation to optimize the size and uniformity of the image in the sample plane. A beam splitter was placed near the focus of the projector lens to direct a small portion of the projector's output onto a monitor detector. The beam splitter (Newport 10Q20RAR.S) was a nanotexture etched fused silica window placed at 45° from the incoming light. The nanotextured coating provided low reflectance over most of the wavelength range of the experiment. After the beam splitter a UV-enhanced aluminum mirror (Newport 5108), at 45°angle of incidence, directed the diffuse light downward to the samples within the sample exposure chamber. The samples were placed on a turntable which rotated during exposures at two revolutions per minute (RPM) to homogenize the dose seen by the samples. A detector and square grid could be placed on top of the sample exposure chamber to facilitate alignment and uniformity scans. This procedure is discussed in Section 3.A.

C. Detectors

Two Gigahertz-Optik detector types were selected to cover the spectral range of 222 to 488 nm. A model UV-3727-5

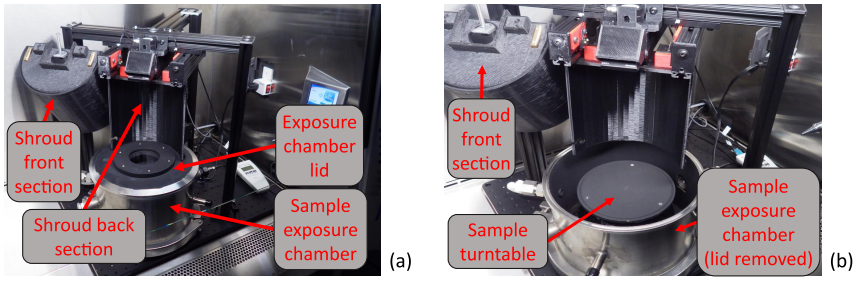

Fig. 4. Photographs of the projector installed in the BSC: the front section of the safety shroud removed to show the sample exposure chamber with (a) the top on the chamber and (b) with the top removed exposing the turntable where the samples were placed.

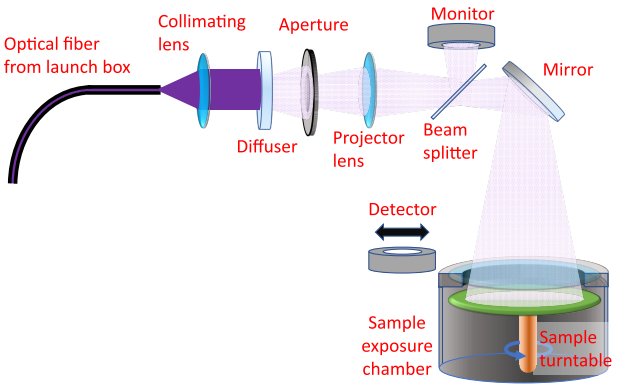

Fig. 5. Projection subsystem optics schematic.

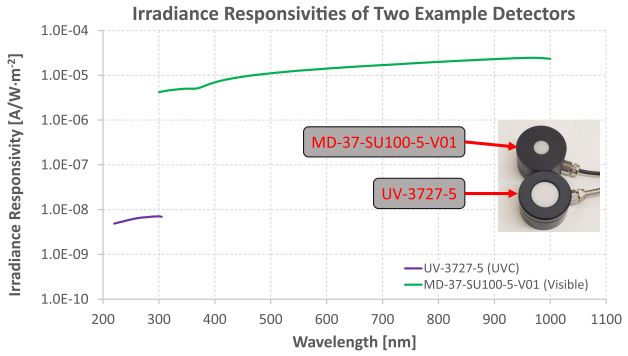

Fig. 6. Example of irradiance responsivities of the detectors. The inset photograph shows examples of the detectors.

UV detector was used for 222 to 305 nm and a model MD-37-SU100-5-VO1 visible detector for 310 to 488 nm. Both detector types were calibrated over a broader spectral range, described below. Two detectors of each type were used with the laser projector, one as the monitor detector and the other as the measurement detector. A Gigahertz-Optik model X1-5 meter was used as the detector measurement device and provided communication to the computer.

As explained above, the BSL-3 lab decontamination would most likely damage the detectors and X1-5 meter. This led to a decision during the system design to use only one Gigahertz-Optik X1-5 meter. Having only one meter required a staff person in the lab to manually switch the measurement and monitor detectors at the meter during the exposure protocol.

D. Detector Calibration

The detectors used in this research were calibrated for irradiance responsivity from 220 to 305 nm for the UV detectors, and from 300 to 1000 nm for the visible detectors. The calibrations were performed in the NIST Automated Pulsed Laser Uniform Source (APLUS) laboratory [11]. The APLUS uses an Ekspla NT242-SH-SFG-SCU 1 kHz optical parametric oscillator (OPO) tunable laser, very similar to the TTLP laser, with a wavelength range from 210 to 2400 nm. The wavelength of the laser is measured with high accuracy using a laser spectrum analyzer. The UV detectors were calibrated against a NIST UV resistant standard detector for irradiance responsivity [12].

Some UV detectors show significant nonlinearity (e.g., 20% difference from a constant responsivity) at low and/or high signal levels; therefore, the detectors were tested for the nonlinearity associated with the level of signal before the calibration, and no obvious nonlinearity was observed within the photocurrent range from 5×10^{-11} A to 1×10^{-8} A, which is a much larger range than that used in this calibration. The detectors were also tested for the nonlinearity associated with the length of integration time. This was also important because the laser has much lower output power in the UV region, and the UV detectors have an irradiance responsivity that was 3 orders of magnitude lower than that of a typical Si photodiode-based radiometer. As a result, the required integration time is quite long (up to 60 s). Nevertheless, no nonlinearity associated with the length of integration time was found in the range from 0.1 to 10 s (or 0.1 to 60 s depending on the detector). The integration time used for this calibration was 10 and 60 s depending on the detector; therefore, no correction is needed for the nonlinearity associated with the length of integration time.

As an example, Fig. 6 shows irradiance responsivities of the UV and visible detectors. The irradiance responsivity expanded uncertainty is estimated to be 3% (with a coverage factor of $k = 2$) for the irradiance responsivity calibration.

E. Software Control

The system is controlled through a computer program that processes the signal from the Gigahertz-Optik X1-5 meter and detectors and controls the exposure shutter. The program can operate in three different modes: irradiance exposure, uniformity, and interactive. In interactive mode, the program is responsive to user input through a graphical user interface. In irradiance exposure mode, the program can control the dose delivered to the test samples either by the dose requested or exposure time input. Since the irradiance level sometimes varied during the day, the exposure time mode was used for the practical reason that the total workday time was predetermined. In uniformity mode the program manually steps through a square grid in the projector beam. The uniformity measurements are described below.

3. PERFORMANCE

A. Uniformity

The system illuminated a 6 cm diameter area with a known irradiance pattern traceable to NIST. The optical modeling showed that the irradiance at the center of the projected beam would be higher than the surrounding area, falling off by 20% near the edge of the illuminated area. Thus, the samples were placed in "rings," which were rotated about the center of the illuminated area with a 2 RPM turntable to provide an optimized uniform irradiance exposure to the samples. Figure 7 shows an average slice of the 253.7 nm irradiance with respect to distance from the center, where the exposure region had an inner radius of 1 cm and an outer radius of 2.5 cm.

The uniformity of the beam on the samples is important. To repeatably measure the uniformity, a square 5 by 5 position grid (18.75 mm center to center spacing) was designed to hold the

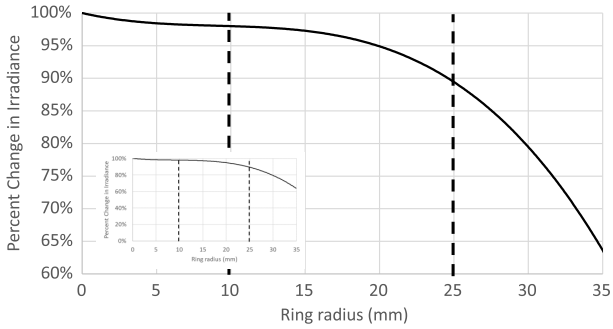

Fig. 7. Solid line is the change in irradiance with respect to ring radius at 253.7 nm. The dashed lines are the inner and outer radius of the exposure area. The inset shows the range from 0% to 100%.

measurement detector in the 25 positions. To ensure the laser projector system performed as expected, the projector beam uniformity was measured on top of the sample exposure chamber in the 5 by 5 grid positions every time the laser wavelength was changed. Before the laser projector was taken into the BSL-3 lab, the projector uniformity was measured in the 5 by 5 grid positions at all experimental wavelengths both on top of the sample exposure chamber and at the sample plane under the sample exposure chamber window. Once installed in the lab, the sample plane measurements are not practically accessible. The uniformity varied slightly with wavelength. Over the duration of the experiment, no change in the projector uniformity per wavelength was observed. Figure 8 depicts examples of the uniformity measured at 222 nm (top), 253.7 nm (middle), and 300 nm (bottom). Contour plots are on the left-hand side, and surface plots are on the right.

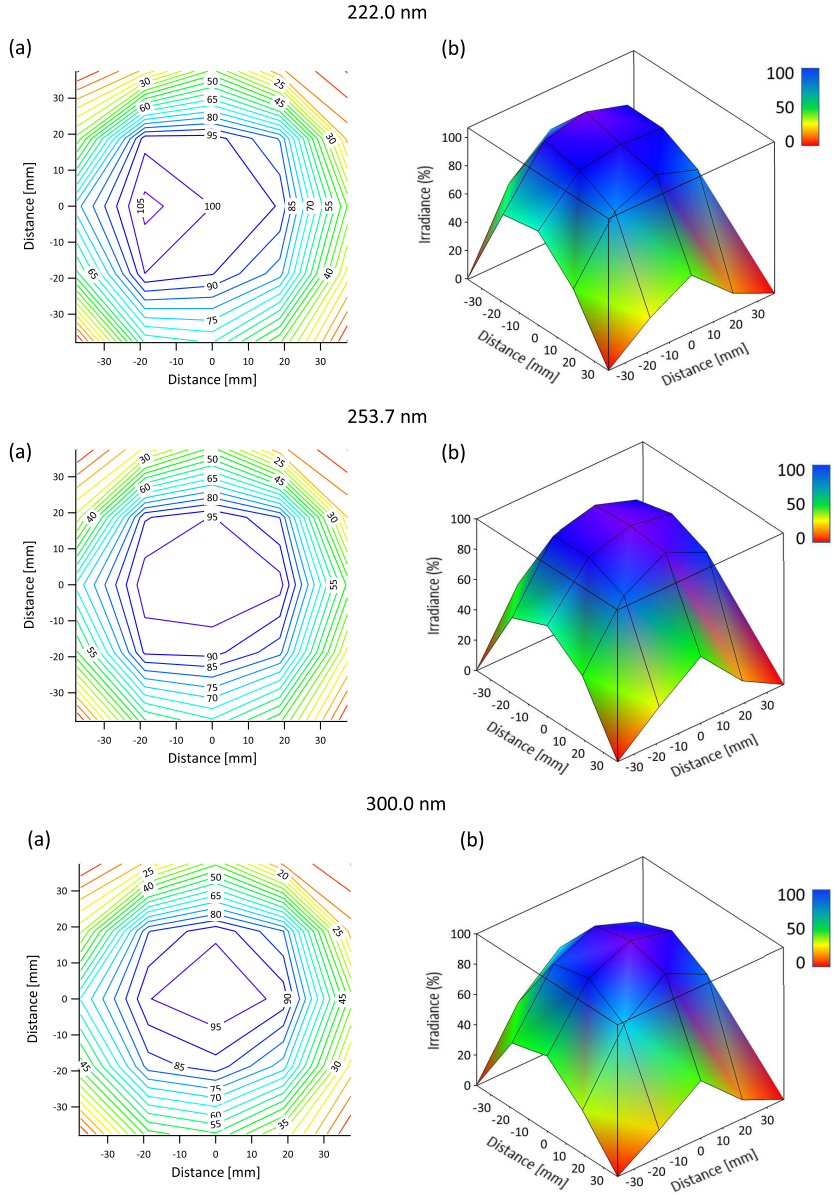

Fig. 8. Example projector beam uniformities at 222 nm (top), 253.7 nm (middle), and 300 nm (bottom). (a) Contour plots are on the left-hand side; (b) surface plots are on the right. All data is normalized to the center position value.

B. Irradiance

In the fields of photobiology and photochemistry, many terms have been used to describe energy interacting with a sample, in this case, a microorganism. Radiant spherical exposure [13,14] or radiant fluence exposure is the quotient of the radiant *energy* of all radiation incident on the outer surface of an infinitely small sphere centered at the specified point and the area of the diametrical cross section of that sphere. The units for radiant spherical exposure are J/m^2. Spherical irradiance [15] or radiant fluence rate is the quotient of the radiant *flux* of all the radiation incident on the outer surface of an infinitely small sphere centered at the specified point and the area of the diametrical cross section of that sphere. The units for spherical irradiance are W/m^2. These are appropriate radiometric quantities for describing the energy interacting with a sample. These quantities are often substituted by radiant exposure or irradiance. Radiant exposure [16] is the density of incident radiant *energy* with respect to area at a point on a real or imaginary surface in units of J/m^2. Irradiance [17] is density of incident radiant *flux* with respect to area at a point on a real or imaginary surface in units of W/m^2. These terms describe the energy available at the surface where the radiation enters the sample media.

The Ekspla NT242-SH-SFG laser system uses several methods from second-harmonic generation to sum frequency generation [18] to produce the different wavelengths. This results in widely varying output powers. Table 1 shows the laser power typically generated for an Ekspla system that is well tuned, and the resulting center point irradiance in the BSC. The expanded uncertainty for the irradiance is 10% ($k = 2$). The fiber input power is calculated from relative measurements comparing the laser output and fiber input at the wavelengths shown. Neutral density filters were required at the laser output for the wavelengths of 405, 450, and 488 nm to ensure the measurement detector operated in its linear regime. The filters were positioned between the exposure shutter and prism. To determine the radiant exposure the irradiance is multiplied by the number of seconds the shutter was opened. Details of the exposure tests can be found elsewhere [19].

Laser power varied with wavelength and tended to drop (with varying rates) during the day due to optical degradation in the laser optics. Additionally, the optical fiber exhibited the effects of solarization [20], which decreased the amount of light reaching the samples. Thus, the time required to achieve the target doses would necessarily increase, especially in the lower UV region (< 250 nm). This was not unexpected and sometimes impacted the actual doses delivered.

The laser wavelength sent to the projector was selected by adjusting the laser output wavelength with its control pad and manually turning the Pellin–Broca prism to optimize the coupling to the optical fiber in the launch box. This required blocking off the laser system in the hallway to keep other people in the area safe from unintentional laser irradiation. Then the laser launch box was opened, and the prism was turned while monitoring for the peak detector signal from the projector output on the sample exposure chamber lid. Also, the laser power was measured at various places in the launch box in order to monitor both the laser and system operation. The time required to tune and measure the laser power and uniformity was the primary reason for the decision to do as many exposures as possible with a single wavelength and made it necessary to work with one wavelength per week.

Each day of operation the measurement and monitor detector signals were recorded, typically twice, once before any sample exposures and again after the sample exposures. The measurement detector was placed at the center position of a 5 by 5 grid on top of the sample exposure chamber. This allowed the ratio of the measurement/monitor detectors (i.e., beam splitter ratio) to be monitored for any changes over time. The ratio stability at each wavelength over the course of this study is shown in Fig. 9.

The signal ratio of the measurement detector on the sample exposure chamber lid and the monitor detector was measured at each wavelength before taking the laser projector system into the BSL-3 lab. These ratios were used as reference ratio values, and the difference between the "daily" measurement/monitor ratios and the reference ratio was monitored. Figure 9 shows the ratio stability by subtracting the mean of the measurement/monitor ratio differences at each wavelength from the individual ratio differences at that wavelength.

Most wavelengths were measured over one week, but some wavelengths were repeated after several weeks, and the control chart shows there was no trending in the ratio values over time. The scatter in the data was similar for all the wavelengths. The scatter is attributed to the laser power stability and the ratio measurement procedure where the measurement and monitor detector signals are measured sequentially (several minutes apart), due to the single meter used in the BSL-3 lab to read the detectors. If two meters were used and sampled simultaneously, as with the APLUS, the scatter in these measurements would be reduced.

Table 1. Typical Laser Power and Irradiance in the BSC

Wavelength [nm]	Laser [mW]	Fiber Input [mW]	Irradiance [$\mu W/cm^2$]	Wavelength [nm]	Laser[mW]	Fiber Input [mW]	Irradiance [$\mu W/cm^2$]
222.0	20	7	3	**300.0**	15	5	47
230.0	30	14	5	**305.0**	30	20	97
240.0	22	12	20	**315.0**	40	23	26
253.7	20	11	30	**325.0**	40	20	26
260.0	17	14	38	**365.0**	22	10	15
270.0	17	10	44	**405.0**	65	22	229
280.0	15	8	32	**450.0**	346	70	487
290.0	11	8	33	**488.0**	350	66	477

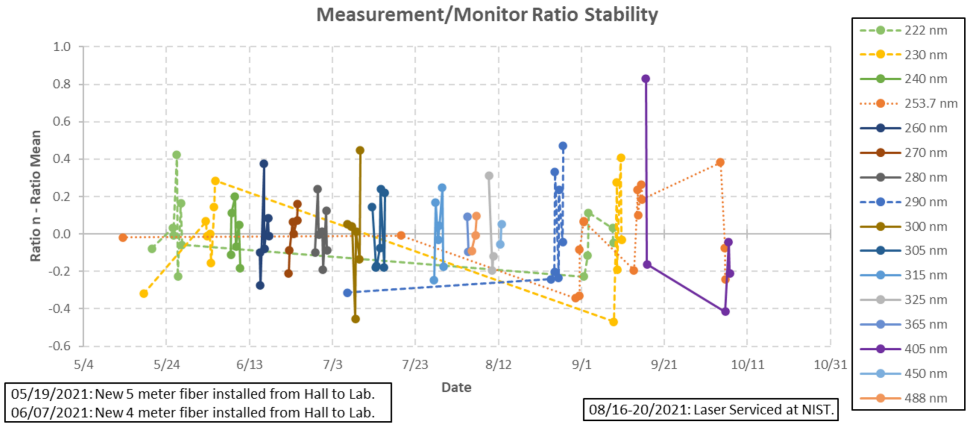

Fig. 9. Measurement/monitor detectors ratio stability chart. Shown are the ratio measurements, typically taken twice a day, over the several months' time of the study. Each wavelength is indicated by a different color. Some wavelengths were repeated after several weeks. The scatter is similar for all the wavelengths The ratio stability data points at each wavelength are determined by subtracting the mean of the measurement/monitor ratio differences from the individual ratio differences at that wavelength.

Also, the laser power level did not change the ratio values, indicating that none of the optical elements in the projection system (after the optical fiber) were being damaged. The laser power varied over the study by 5× or greater at several wavelengths, especially after the laser was serviced. And the laser power at some visible wavelengths is an order of magnitude greater than the UV. As expected, the three fibers used did not affect the projector ratios.

As stated above, the monitor detector and measurement detector signals on the top of the sample exposure chamber lid and at the sample plane were measured before the projector was taken into the BSL-3 lab. This could not be repeated during the 6 months of this study due to the impracticality of changing the physical setup to take measurements at the sample plane. However, after all the exposures were taken, the setup was modified to take measurements of the monitor detector and the measurement detector both on top of the sample exposure chamber lid and at the sample plane. Figure 10 shows the measurements before and after the sample exposures. The difference shows that the sample exposure chamber window did not change during the 6 months of operation. The small difference is affected by the relatively large uncertainty in the first measurements.

As expected in the UVC wavelength range, the fiber suffered from solarization. Figure 11 shows the solarization effects for three consecutive days of exposure at 222 nm. The effect of solarization appeared to be very minor (6% drop) at 270 nm with a significant (50% drop) at 222 nm. The fiber transmission would recover slightly between days but then would quickly approach an asymptote.

4. CONCLUSION

In response to the COVID-19 crisis, the National Institute of Standards and Technology designed, built, and deployed a tunable laser projection system, and in conjunction with the National Biodefense Analysis and Countermeasures Center, studied the inactivation of SARS-CoV-2 due to exposure to different UV and blue light wavelengths. The laser and projector system design and performance over the wavelength range of 222 to 488 nm were presented. This system can be replicated or

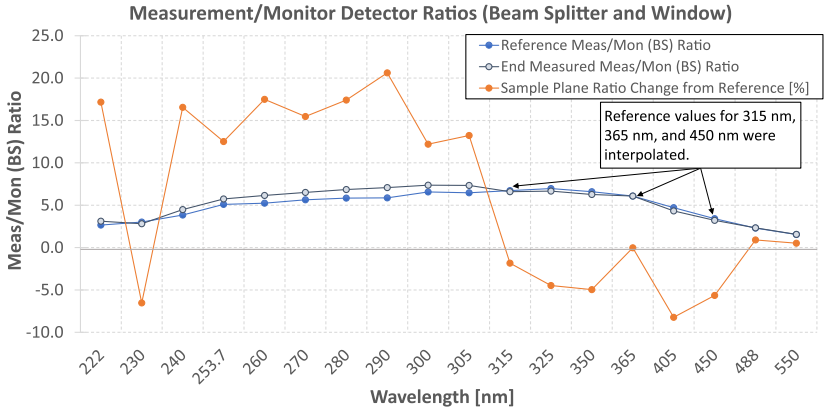

Fig. 10. Measurement/monitor ratios at the beginning and end of the study. The monitor detector and measurement detector signals on the top of the exposure chamber lid and at the sample plane were measured before the projector was taken into the BSL-3 lab and after all the exposures were taken. The ratios show that the exposure chamber window did not change during study. The difference is due to the uncertainties in the first measurements.

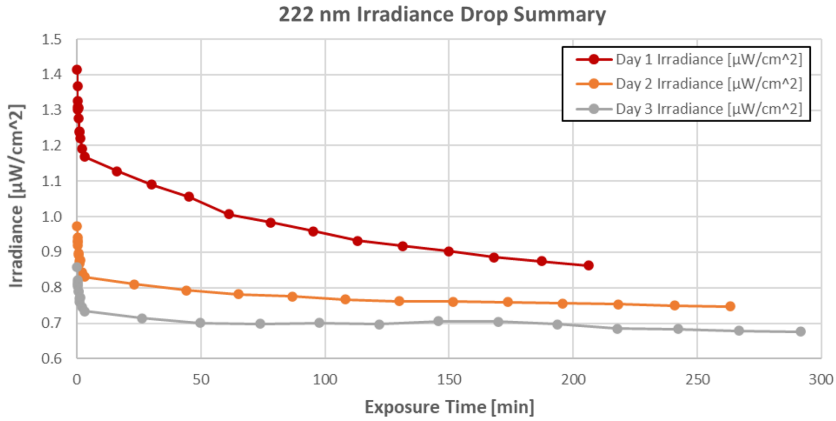

Fig. 11. Degradation of the fiber due to solarization when exposed to the 222 nm UV radiation on three consecutive days.

modified for similar applications. And most importantly, the results of this comprehensive wavelength study indicate that UV radiation can inactivate SARS-CoV-2 and can serve as a baseline for further studies.

Funding. U.S. Department of Homeland Security (DHS) Science and Technology Directorate (ST) (HSHQDC-15-C-00064).

Acknowledgment. The authors thank their NIST colleague, Catherine Cooksey, for the reflectance and transmittance measurements of several materials used in this study.

This work was supported by the NIST and by the DHS Science and Technology Directorate (Battelle National Biodefense Institute for the management and operation of the National Biodefense Analysis and Countermeasures Center, a Federally Funded Research and Development Center).

Disclaimer. Certain commercial equipment, instruments, or materials are identified in this paper to foster understanding. Such identification does not imply recommendation or endorsement by the National Institute of Standards and Technology or the Department of Homeland Security, nor does it imply that the materials or equipment identified are necessarily the best available for the purpose.

Disclosures. The authors declare no conflicts of interest.

Data availability. Data underlying the results presented in this paper are not publicly available at this time but may be obtained from the authors upon reasonable request.

REFERENCES

1. Centers for Disease Control and Prevention (CDC), "Healthcare-associated infections: HAI data and statistics, 2018," (2018).
2. Joint Hearing Before the Subcommittee on Research and Technology & Subcommittee on Oversight Committee on Science, Space, and Technology, (SRT&SOCS), "Technology for patient safety at veterans' hospitals," in *113th Congress, 2nd Session, Serial No. 113-83* (U.S. House of Representatives, 2014), p. 12.
3. Centers for Disease Control and Prevention (CDC) and National Center for Health Statistics, "Health, United States, 2016: with chartbook on long-term trends in health," 2017, https://www.cdc.gov/nchs/data/hus/hus16.pdf.
4. K. P. Hartnett, A. Kite-Powell, J. DeVies, M. A. Coletta, T. K. Boehmer, J. Adjemian, and A. V. Gundlapalli, "Impact of the COVID-19pandemic on emergency department visits-United States, January 1, 2019–May 30, 2020," Morbidity and Mortality Weekly Report 69 (2020), p. 699.
5. M. P. Stevens, M. Doll, R. Pryor, E. Godbout, K. Cooper, and G. Bearman, "Impact of covid-19 on traditional healthcare-associated infection prevention efforts," Infect. Control Hosp. Epidemiol. **41**, 946–947 (2020).
6. J. R. Bolton and C. A. Cotton, *The Ultraviolet Disinfection Handbook* (American Water Works, 2011).
7. M. Masjoudi, M. Mohseni, and J. R. Bolton, "Sensitivity of bacteria, protozoa, viruses, and other microorganisms to ultraviolet radiation," J. Res. Natl. Inst. Stand. Technol. **126**, 1–77 (2021).
8. J. R. Bolton and K. G. Linden, "Standardization of methods for fluence (UV dose) determination in bench-scale UV experiments," J. Environ. Eng. ASCE **129**, 209–215 (2003).
9. T. C. Larason, "National institute of standards and technology transportable tunable ultraviolet laser irradiance facility for water pathogen inactivation," Rev. Sci. Instrum. **91**, 074105 (2020).
10. W. McClain, "How to mount a pellin-broca prism for laser work," Appl. Opt. **12**, 153 (1973).
11. Y. Zong, S. W. Brown, G. P. Eppeldauer, K. R. Lykke, and Y. Ohno, "A new method for spectral irradiance and radiance responsivity calibrations using kilohertz pulsed tunable optical parametric oscillators," Metrologia **49**, S124–S129 (2012).
12. U. Arp, E. Hagley, and R. Vest, "Eliminating the middleman: ultraviolet scale realization using a laser-driven plasma light source," Appl. Opt. **60**, 1729–1736 (2021).
13. International Commission on Illumination (CIE), "e-ILV, International Lighting Vocabulary, 2nd edition, CIE S 017:2020," 2020, https://cie.co.at/e-ilv.
14. International Commission on Illumination (CIE), 2020, https://cie.co.at/eilvterm/17-21-074.
15. International Commission on Illumination (CIE), 2020, https://cie.co.at/eilvterm/17-21-054.
16. International Commission on Illumination (CIE), 2020, https://cie.co.at/eilvterm/17-21-071.
17. International Commission on Illumination (CIE), 2020, https://cie.co.at/eilvterm/17-21-053.
18. Ekspla, *Ekspla NT242-SH Technical Description and User's Manual* (2010).
19. Publication by M.A. Schuit accepted for publication (2022).
20. E. J. Friebele, "Optical fiber waveguides in radiation environments," Opt. Eng. **18**, 552–561 (1979).